Shadow Detection via Morphological Filtering and Paired Regions Based Learning: A Review

Deepika Digarse[1], Krishna Chauhan[2]
1. M. Tech student in Sagar Institute of Research and Technology Bhopal, India
2. Assistant Professor ECE Department in Sagar Institute of Research and Technology Bhopal, India

Abstract*—The shadows in high-resolution satellite images are usually caused by the constraints of imaging conditions and the existence of high-rise objects. This is particularly so in urban areas. The paired region based method explores pixel or edge information; we employ a region-based approach. In accumulation to considering individual regions singly, we predict relative illumination conditions between segmented regions from their appearances and perform pair-wise classification based on such information. Classification results are used to build a graph of segments, and graph-cut is used to solve the labelling of shadow and nonshadow regions To alleviate the shadow effects in high-resolution images for their further applications, this paper proposes a novel shadow detection algorithm based on the morphological filtering and a novel shadow reconstruction algorithm based on the example learning method. In the shadow detection stage, an initial shadow mask is generated by the thresholding method, and then, the noise and wrong shadow regions are removed by the morphological filtering method. Experimental results on Quick Bird and WorldView-2 satellite images have demonstrated that the proposed shadow detection algorithm can generate accurate and continuous shadow masks and also that the estimated nonshadow regions from the proposed shadow reconstruction algorithm are highly compatible with their surrounding nonshadow regions. Finally, we examine the effects of the reconstructed image on the application of classification by comparing the classification maps of images before and after shadow reconstruction.

Index Terms*—Example learning, Markov random field (MRF), morphological filtering, shadow detection, shadow reconstruction.

I. INTRODUCTION

SHADOWS, created wherever an object obscures light source, are an ever-present aspect of our visual experience. Shadows can either aid or confound scene interpretation, depending on whether we model the shadows or ignore them. If we can detect shadows, we can better localize objects, infer object shape, and determine where objects contact the ground. Detected shadows also provide cues for lighting conditions [2] , about scene geometry [3]. But, if we ignore shadows, spurious edges on the boundaries of shadowed surface and confusion between albedo and shading can lead to mistakes in visual processing. For these reasons, shadow detection has long been considered a crucial component of scene interpretation (e.g., [4], [5]).

The goal of PR based shadow detection is to detect shadows in from the images. To determine whether a particular region is shadowed, we compare it to another area of image that are likely to be of the same material. To start, we find pairs of regions that are likely to correspond to the same material and determine whether those are having equal lighting (illumination) conditions. We incorporate these pairwise relationships together with region-based appearance features, in a shadow/ nonshadow graph. The node potentials in our graph encode region appearance; a sparse set of edge potentials indicate whether two regions from the same surface are probably to be of the same or different illumination. Finally, the regions are jointly classified as shadow/nonshadow by means of graph-cut inference. Like Zhu et al. [1] and Lalonde et al. [6], we take a data-driven approach, learning our classifiers from training data, which leads to good performance on consumer-quality photographs. Unlike others, it explicitly models the material, illumination relationships of pairs of regions, including nonadjacent pairs.

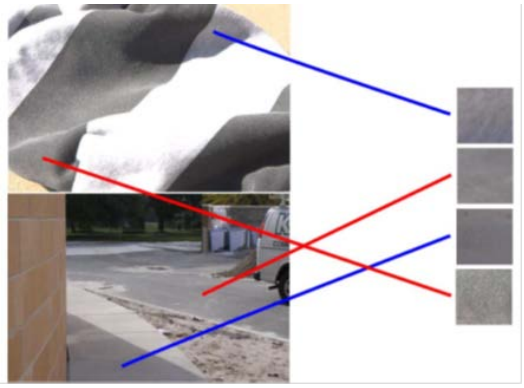

Fig. 1. What is in shadow? Local region appearance can be ambiguous; to find shadows, we must compare surfaces of the same material [29].

By modelling long-range interactions, we are planning for detect soft shadows, which may be difficult to detect locally. By restricting comparisons to regions with the same

substance we intend to develop robustness in complex scenes, material and shadow boundaries perphaps coincide [29]. Paired region based shadow detection provides binary pixel labels, but shadows are not truthfully binary. Illumination often changes gradually across shadow boundaries.

WITH the technological developments in aerospace, an increasing number of Earth observation commercial satellites with high-resolution sensors have been launched, such as Quick Bird (QB), IKONOS, World View-2 (WV-2). Image obtained from such kind of satellites have very high spatial resolution (VHSR), usually ranged from 0.5 to 4 m. At this resolution, details such as buildings and other infrastructures are easily visible. Therefore, these VHSR images have opened a new era for remote sensing applications, e.g object detection [7], and classification [8], object mapping [9], and change recognition. In particular, VHSR images have dragged interest of researchers studying city areas, because of the existence of relatively small features, like houses, tree, mall etc. Inevitably, tall standing objects (which mainly are mall) among these small features cast long shadows in most of the captured VHSR images. On the one hand, these shadows may be utilized as a valuable cue for inferring 3-D scene information based on their position, shape and size like for any building 0r mall detection and its height estimation [10]. On the other hand, the shadows are the reason partial or total loss of radiometric information in the affected areas, and consequently, they are the cause of making task difficult to solve like image interpretation, object detection and recognition, and change detection or I can say it may be impossible to find out [11]. In this paper, we focus on the second aspect of shadows, i.e., to attenuate the problems occurred by the loss of radiometric information in shaded areas by compensating or reconstructing them. Generally, two steps are involved in this procedure: 1) shadow detection and 2) shadow reconstruction (compensation). Regarding shadow detection in VHSR images, two main approaches are reported in the previous literature, namely, the model-based and the property-based. The former requires prior knowledge of scene or sensors, including, without limited to, distribution of scene radiance and acquisition parameters like sun azimuth, sensor/camera localization, date, and the time of day of acquirement. On the basis of previous information, model-based approaches are attain improved performance in detecting a particular type of objects like buildings and automobiles [12], [13]. Conversely, these approaches are may be not general enough for dealing with the great diversity of geometric structures which usually exist in VHSR satellite images of urban areas. The property-based approaches make use of firm shadow properties in images, such as brightness, spectral characteristics, and geometry. Because of their simplicity both in principle and implementation, the property-based approaches have been widely used in literature; they generally include four (usually interrelated) categories: 1) thresholding-based; 2) color-transformation-based; 3) region-growing-based; and 4) classification-based. In the thresholding-based methods, the shadow and nonshadow pixels are determined according to a predefined threshold level, which normally set as per the bimodal distribution of image histogram, such as the method in [11]. In the color-transformation-based methods, the red–green–blue (RGB) color image is first transformed to a 3-D space, such as hue–intensity–saturation, hue–saturation–value (HSV), and Yc_bc_r models; followed by, a new image is imitative according to specific spectral properties of shadows in new room, like shadow areas having inversely proportional relationship in between intensity and hue, saturation.[14]; finally, shadows are detected by thresholding the derived new image. The proposed shadow detection method in [15] first transformed the true color image into HSV space and then derived a normalized saturation–value difference index (NSVDI) to identify shadows via thresholding. numerous photometric invariant color models for shadow detection were compared in [16]. The authors in [18] proposed a linear regression method to bridge nonshadow and shadow areas for each class in each band. In present work, one more linear-regression-based method which can be applicable shadow reconstruction has been proposed in [17], which assumed that both shadow and nonshadow pixels of each class follow a Gaussian distribution and then solved the linear regression parameters by the parametric estimation method. The problem with these linear regression methods is that they lost local unpredictability for each class due to the implementation in a global manner. Clearly, all the aforementioned methods for shadow reconstruction are based on classification thus need to determine the class of the shadowed areas before reconstruction. In the algorithm proposed in [17], the first step was to collect ground-truth region pairs for all classes, i.e., nonshadow classes and their shadow counterparts; then, these ground-truth regions were utilized for supervised classification in shadow and nonshadow classes separately. In the shadow reconstruction method proposed in this paper, a similar ground-truth collection course of action will be adopted but without the classification step. In this paper, we propose an alternative shadow detection algorithm based on thresholding and morphological filtering, together with an alternative shadow reconstruction algorithm based on the eg. learning method and Markov random field (MRF). During the shadow detection modus operandi, the bimodal

distributions for pixel values in the near-infrared (NIR) band and the panchromatic band are adopted for thresholding. During the shadow reconstruction procedure, we model the relationship between nonshadow and the corresponding shadow pixels and between neighbouring nonshadow pixels by employing MRF.

II. SHADOW DETECTION

To detect shadows, we must consider the appearance of the local and surrounding regions. Shadowed regions are about to be dim(dark or shaded), with little bit texture, but some non-shadowed regions may have comparable characteristics. Surrounding regions that correspond to the same material can provide much stronger evidence; For example, suppose regions_i is comparable to s_j in texture and (color property) chromaticity. If s_i has similar intensity to s_j , then they are probably under the same illumination and should receive the same shadow label (either shadow or nonshadow). However, if s_i is darker than s_j, thens_i probably is in shadow and s_j probably is not. We first segment the image using the mean shift algorithm [19]. Subsequently, applying trained classifier, we estimate confidently that each region is in shadow. We also find the equal value illumination pairs and different illumination pairs of regions, which are confidently predicted to correspond to the same material and have either similar or different illumination, respectively. We construct a relational graph using a sparse set of confident illumination pairs. Finally, we solve for the shadow labels y ¼ fig 1; 1gn (1 for shadow) that maximize the following objective:

$$\hat{y} = \underset{y}{\arg max} \sum_{i=1} c_i^{shadow} y_i + \alpha_1 \sum_{\{i,j\}\epsilon E} C_{i,j}^{diff} (y_i - y_j) - \alpha_2 \sum_{\{i,j\}\epsilon E_{same}} C_{ij}^{same} \; 1 (y_i \neq y_j) \quad (1)$$

wherec_i^{shadow} is the single-region classifier confidence weighted by region area, fig.2 E_{diff} are different illumination npairs, fig. 2E_{same} are equal illumination pairs C_{ij}^{same} and $C_{i,j}^{diff}$ are the area-weighted confidences of the pairwise classifiers, 1 and 2 are parameters, and 1ð:Þ is an indicator function. In the following sections, we describe the classifiers for single regions (Section 2.1) and pairs of regions (Section 2.2) and how we can reformulate our objective function to solve it efficiently with the graph-cut algorithm (Section 2.3).

2.1 Single-Region Classification

When a region becomes shadowed, it becomes darker and less textured (see [1] for empirical analysis). Thus, the color and texture of a region can help predict whether it is in shadow. We symbolize color with a histogram in “L*a* b” space, along with 21 bins per channel. We represent texture with the texton histogram with 128 textons, provided by Martin et al. [20]. We train our classifier from manually labelled regions using an SVM with a kernel (slack parameter C ¼ 1) [21]. We define C_{shadow}^{i} as the log likelihood output of this classifier times a_i , the pixel area of the i^{th}region.

2.2 Pairwise Region Relationship Classification: is in shadow by considering only its internal appearance; we must compare the region to others with the same material. In particular, we want to find identical illumination pairs, regions with same material, lightning and having equal illumination and vice versa. Differences in illumination are caused by straight light blocked due to other things, self-shading, or by dissimilarity in surface orientation. Comparison between regions with different materials is uninformative because they have different reflectance. We detect shadows using a relational graph, with an edge connecting one and all illumination pair. To better handle occlusion and to link similarly lit regions that are divided by shadows; we enable edges between regions that are not adjacent in the image. Because of the reason of having many pairs of regions are not of same material, Of graph is still very sparse. Examples of such relational graphs are shown in Fig. 3. When regions are off the record as having dissimilar illuminations the shadowed region is specified. We train classifiers (SVM with RBF kernel; C ¼ 1 and ¼ 0:5) to detect lighting pairs based on comparisons of their color and texture histograms, is the ratio of their lightning condition (intensities), and their chromatic alignment, and their distance in the image. These features encode the intuition that regions of the same reflectance share similar texture and color distribution when viewed under the same illumination; when viewed under different illuminations, they tend to have similar texture but differ in color and intensity.

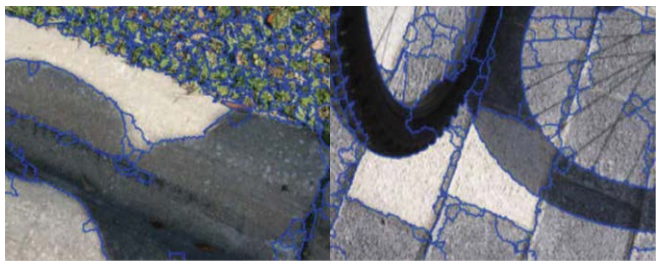

Fig. 2. Illumination relation graph of two example images. Green lines indicate same illumination pairs, and red/white lines mean different

illumination pairs, where white ends are the nonshadow regions and dark ends are shadows. The width shows the confidence of the pair [29].

It is taken into explanation the distance between two regions, which greatly reduces false comparisons while enabling flexibility in comparison of considering only adjacent pairs. The distances between color and texture histogram is computed as in Section 2.1. We also work out normalized texton histogram, where we standardize the sum of filter responses at each pixel to 1. Regions of having equivalent material will repeatedly have analogous texture histograms, apart from of differences in shading. When regions have both similar color and texture, they are likely to be same illumination pairs. Ratio of true color (RGB) average intensity are calculated as ð_R ¼

$$\frac{R_{avg\,1}}{R_{avg\,2}}, \rho G = \frac{G_{avg\,1}}{G_{avg\,2}}, \rho B = \frac{B_{avg\,1}}{B_{avg\,2}}$$

Here$R_{avg\,1}$, for example, is the average value of the red channel for the first region. For a shadow/non shadow pair of the same material, the non shadow region has a higher value in all three channels; Chromatic arrangement. Studies have shown that color of shadow/non shadow pairs tend to align in true color space [22]. Simply put, the shadow region should not look more red or yellow than the non shadow region since direct light usually has a higher color temperature than the ambient light (e.g., the sun is yellow and the sky is blue). This ratio is computed as _R=_B and _G=_B. Normalized distance in position. Because distant image regions are less likely to correspond to the same material, we also add the normalized distance as a feature, computing it as the Euclidean distance of the region centres divided by the square root of the geometric

$$\text{areas:}\widehat{D}\left(R_i, R_j\right) = \frac{D(R_i, R_j)}{\sqrt{a_i^{1/2}}, a_j^{1/2}}$$

mean of the region We define C_j^{same} as the log likelihood output of the classifier for same-illumination pairs times ffia $a_{i,j}$ P , the geometric mean of the region areas. Similarl

y, $C_{i,j}^{diff}$ is the log probability output of the classifier for different illumination pairs epoch $a_{i,j}$ p. Edges are weighted by region area and classifier score so that larger regions and those with more confidently predicted relations have more weight.

Note that the edges in E_{diff} are directional: They persuade y_i to be shadow and y_j to be nonshadow. In the pair-wise categorization, apiece pair of regions is labeled as different illumination, same illumination, or different material, either is most confident. Regions of different material pairs are not directly connected in the graph. If there are many edges, to make the inference procedure faster we include the top 100 most confident boundaries, which empirically yield very similar results.

2.3 Graph-Cut Inference

We can apply competent and finest graph-cut inference by reformulating our objective function (1) as the following

Energy minimization:

$$\hat{y} = arg_y\ min \cos t_k^{unary}\ (y_k) + a_2 \sum_{(ij)\epsilon E_{max}} c_{ij}^{same}\, 1(y_i \neq y_j \quad (2)$$

With

$$\cos t_k^{unary}\ (y_k) = -c_k^{shadow}\, y_k - \alpha_1 \sum_{\{i=k,j\}\epsilon E_{diff}} c_{i,j}^{diff}\ y_k + \alpha_1 \sum_{\{i=k,j\}\epsilon E_{diff}} c_{i,j}^{diff}\ y_k \quad (3)$$

Because this is customary (binary, with pair-wise term encouraging affinity), we can solve for $\hat{y}$ using graph cuts [23]. In our experiments, eqn 1 and eqn 2 are determined by cross legalization on the training set. We set eqn1 ¼ 1 and eqn 2 ¼ 2.

III. MORPHOLOGICAL FILTERING METHOD

The flowchart in Fig. 3 shows the principal steps of the proposed methodology. The whole method includes shadow recognition and shadow reconstruction stages by executing on a multispectral (MS) satellite image of an urban area scene.

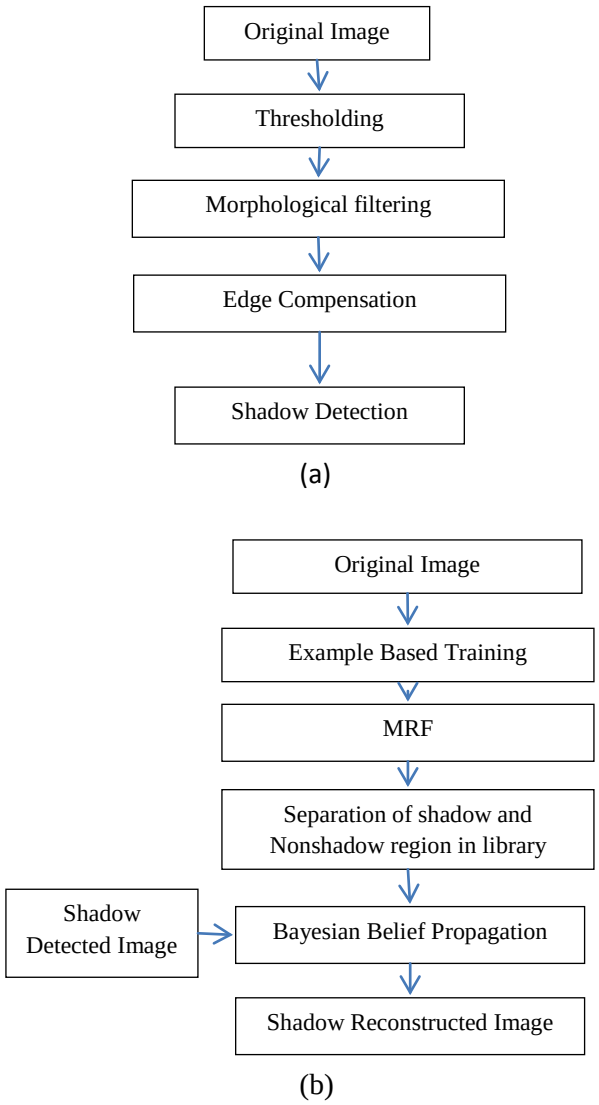

Fig. 3. Flowchart of the MF based method (a) shadow detection (b0 shadow removal [30].

The main role of this paper in the shadow detection stage is that we join thresholding and morphological filtering techniques by making an allowance for the spectral characteristics of diverse land-cover types. The shadow recognition stage consists of three main steps: thresholding, morphological filtering, and boundary reimbursement. The main dilemma i.e. penumbra effect will be handled by shadow perimeter reimbursement in the MF shadow detection algorithm. Here first it is gives the fundamental steps in the shadow region of the image. For a given shadow region *Rs* on a VHSR image, we seek to estimate the corresponding non shaded region R_n This problem can be formulated as a maximum *a posterior* problem, i.e., $P(R_n|R_s)$ finding R_n that maximizes posterior probability), which is expressed as:

$$\hat{R} = arg_{R_n} \max P(R_n|R_s) \quad (1)$$

According to the Bayesian theorem, $P(R_n|R_s)$can be expressed as

$$P(R_n|R_s) = {P(R_s, R_n)}/{P(R_s)} \quad (2)$$

where $P(R_n|R_s)$is the joint probability of R_s and R_n and is $P(R_s)$a prior probability of R_s. Since $P(R_s)$ is a constant over nonshadow pixels, (1) we can equivalently written as:

$$\widehat{R_n} = arg_{R_n} maxP(R_s, R_n) \quad (3)$$

The research in [18] indicated that the darkness of shadow depends heavily on the bordering conditions. Therefore, it is necessary to build multiple affairs for every one nonshadow class and its shadowed counterpart in one scene. In this paper, this problem is treated by manually collecting nonshadow and shadow pixel pairs in different locations of one scene for each class during the training procedure. Because of the reality of human interaction, one requirement for the MF based shadow reconstruction algorithm is that the shadowed areas in the studied VHSR satellite image are not so dark, thereby enabling human eyes to distinguish the classes under shadowed pixels. In the case that the shadowed areas are so dark, one possible solution is to find a reference image with little or without shadows to assist in the training process.

Here it is describing the step by step procedure in detail. First, a preliminary darkness facade is unoriginal by the thresholding method according to the spectral characteristics of the MS image. After that, shadow masks are elaborated by morphological operations to filter noise, wrong shadow areas. At long last, the shadow edges are compensated considering the effects of penumbra and the surrounding conditions of shadows on VHSR images. The shadow reconstruction stage includes two main steps: example-based training and shadow reconstruction via Bayesian belief propagation (BBP); sooner than the preparation step, the nonshadow and shadow samples are first collected from the same image scene manually by visual judgment. Then, the training samples formulate a nonshadow library and a shadow library, which are correlated with an MRF. With the trained nonshadow and shadow libraries, the underlying nonshadow pixels can be reconstructed from the corresponding shadow pixels according to the derived shadow mask in the shadow detection stage.

3.1 Thresholding for Shadow Detection

Since the NIR spectrum has higher reflectivity than visual spectrum for many urban land-cover types, the digital number (DN) values of urban VHSR images are higher in the NIR band than in other bands. For shadow areas, the DN values in an NIR band drop in a higher degree because of the occlusion of direct sunlight. The study in [18] has shown that the DN ratio of light shadow and sunlight is lower in NIR band than in true color bands. In this paper, we compare the ratios of nonshadow and shadow pixel values in different bands of QB andWV-2 images, which will be studied in our tentative part. We selected four common land-cover types in urban areas as the study objects hereof: building, lane, and concrete. The nonshadow and the corresponding shadow samples (collected for training in step of constructing learning model in Section III-D) for the same objects (class) are first averaged, respectively, and subsequently, the ratios of non shadow and shadow values are imitative for each land-cover type. The curves of ratio with respect to band number from which we can observe that the non shadow and shadow ratios in the NIR band are the peak for all land-cover types both on the QB image (band 4) and the WV-2 image (bands 7 and 8). These indicate that it is the easiest way to distinguish shadow areas in the NIR band than in other bands. We thus execute the thresholding algorithm in the NIR band for shadow detection. Because there are mainly two features of interest, i.e., shadows and non shadows, and there exists a gap in their DN values, we assume that there are two main modalities in the NIR histogram. The threshold level can then be unwavering by the bimodal histogram splitting method [24]. The threshold level T is set to the mean of the two peaks in the NIR histogram [11], which was found by experiments to give every time exact threshold levels in separating the shadow from the nonshadow regions. The shadow mask is then derived by the following formula:

$$M_T = \begin{cases} 1, & if\ DN_{NIR} > T \\ 0, & else \end{cases}$$

As the study scene may contain objects that have very low values in the NIR band but high values in other bands, such as water having relative high values in the green band, the derived shadow mask from the NIR band is further refined by the thresholding results in other bands (in this paper, we use the panchromatic band, which is approximated by the average of all other bands in the visual spectrum), i.e., if the detected shadow pixel in the NIR band is judged to be a nonshadow pixel in the panchromatic band, then this pixel is set to be a nonshadow pixel in the final shadow mask.

3.2 Morphological Filtering for Shadow Detection

An example of a shadow mask derived from the thresholding method is shown in Fig. 3(b), with black indicating shadow pixels and white indicating non shadow pixels. From this, we can observe that there are two problems: 1) the existence of many small discontinuous shadow regions caused by the salt and pepper noise in VHSR images and 2) the wrong shadow regions caused by the low DNs of some objects both in the NIR and the panchromatic bands, particularly roads. In order to keep the shape of the detected shadow regions and to remove the noise, we adopt the morphological image processing method to enhance the detected shadow mask M_T derived from the thresholding method. Moreover, the morphological operations can remove the wrong shadow regions with appropriate prior information. Mathematical morphology is a set- and lattice-theoretic methodology for image analysis, which aims to quantitatively describe the geometrical structure of image objects [25]. Thus, morphological filters, which are more suitable than linear filters for shape analysis, play a major role in geometry-based enhancement and detection. The basic morphological operations include erosion and dilation. With a structuring element, erosion shrinks the object, and dilation grows the object. When combining erosion and dilation, two new operations are generated, that is to say, opening (erosion followed by dilation) and closing (dilation followed by erosion), which keep the general shape of objects but possess different smoothing effects. Specifically, opening removes small protrusions and thin connections, whereas the closing fills in small holes. In this paper, we adopt opening and closing operations to remove the noise and wrong shadows in M_T with a structuring element of 3 × 3 ones. Because the shape of roads is usually thin, the opening operation is applied to M_T once. Consequently, the road shadows are broken into discrete small regions, which can be deemed as noise in further steps. For illustration, the enhanced mask M_{To} of example M_T in Fig. 3(b) after this opening operation is shown in Fig. 3(c). To remove the noise in nonshadow areas, one opening operation with an eight-connected vicinity constraint and area specifications is applied to M_{TO} based on the following steps: 1) determining the connected components; 2) computing the area of each component; and 3) removing small regions whose areas are smaller than a predefined threshold *At*. The enhanced mask M_{TOO} of example M_{TO} in Fig. 3(c), after this step has been carried out, can be seen in Fig. 3(d). To remove the noise in shadow areas, the closing operation is applied to M_{TOOC} with the same procedures as in the aforementioned opening operation. The enhanced shadow mask M_{TOOC} of M_{TOO} in Fig. 3(d); after this step is shown Fig. 3(e). The two predefined thresholds in the aforementioned opening and closing operations should vary

according to different spatial resolutions of study images. There are two solutions for this problem:

1) They can be determined empirically by experiments, and 2) they can be determined by some prior knowledge, for example, the smallest possible shadow area can be determined by the prior information about the high rise objects in the study scene. We adopt the first strategy in this paper. Since the noise regions from broken roads are larger than those in shadow areas, the predefined thresholds in the aforementioned opening and closing operations can be set larger and smaller accordingly, for example, $A_t = 80$and $A_t = 30$ and for deriving shadow masks in Fig. 3(d) and (e), respectively. For those thin shadows caused by bridges, we can first become aware of the bridges by adopting relevant methods [26] ; then keep such shadows in the final shadow mask by considering their spatial locations with the detected bridges.

3.3 Shadow Edge Compensation

The width of the penumbra varies with the changes in the elevation angle of the sun and the height of the objects. For simplicity, the penumbra effect is tackled by compensating one pixel at the shadow edges. However, for shadow areas whose backdrop are high-brightness areas, their shadows edges are affected, and hence, the penumbra width needs to be extended in this case. It compensates these shadow edges by conducting the following steps: 1) growing both high-brightness and shadow areas along back-light and to-light directions, correspondingly, by a dilation operation, and 2) taking their intersecting regions as the compensated shadow edge regions.

3.4 Learning Model of Shadow and Nonshadow Pixels Based on MRF

With light shadows in the VHSR image, we first extract shadow and non shadow pixel samples in the study scene for training purposes. During this procedure, two conditions need to be satisfied: 1) The non shadow and corresponding shadow samples for one land-cover type are as close as possible in spatial location to alleviate the effects of surrounding condition and illumination variation, and (2) the sampled shadow and non shadow pixel pairs should include all land-cover types that may incur shadows in the study scene. With proper discrimination capability, this collection procedure is fast, and the time taken varies with the size of a study scene (a larger study scene costs longer time and vice versa). Because of the complexity of imaging conditions and illumination variations in satellite sensors, it is knotty to build the relationship between shadow and nonshadow pixels with linear estimation methods. We thus relate shadow and non shadow pixels by employing an MRF due to its good performance at modelling spatial relationships, such as in remote sensing applications of object identification [27] and image segmentation [28]. Then we make the following Markov assumptions:

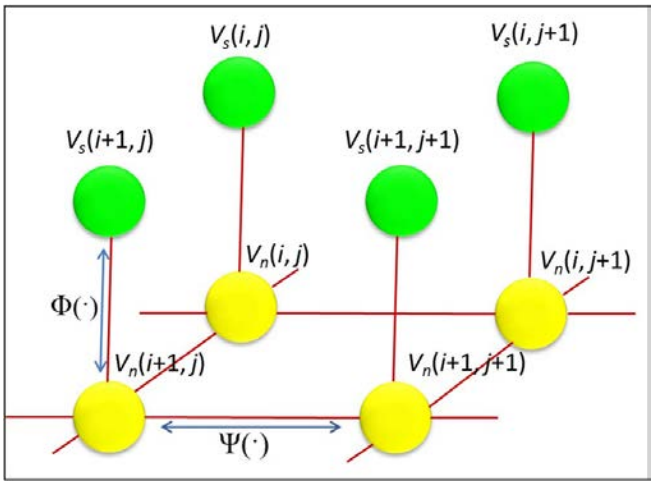

Fig. 4. MRF model for shadow and nonshadow PVs.

Each node in the network denotes a PV of shadow or nonshadow areas. Lines of the graph point towards statistical dependences among nodes.

For every shadow and underlying non shadow pixels, these are assigned to one node of a Markov network; each node is statistically free from another node apart from its direct neighbour. For a VHSR image with B-bands, a shadow pixel vector (PV) is denoted as Vs $\in$ RB (i.e., the pixel standards on all bands) and underlying non-shadow PV as $V_n \in RB$. We connect each non-shadow PV both to its corresponding shadow PV and to its spatial neighbours, as the example with four pixels shown in Fig. 4. Each non-shadow PV $V_n(i,j)$ is related to its analogous shadow PV$V_s(i,j)$; its neighbours$V_n(i+1,j)$,$V_n(i,j+1)$, $V_n(i-1,j)$, and $V_n(i,j-1)$. The relationship between these nodes can be represented by $\Theta(\cdot)$ and $\Psi(\cdot)$, correspondingly. $\Theta(\cdot)$ is the compatibility function of V_n and its correspondingV_s, and $\Psi(\cdot)$ is the compatibility function of $V_n$and its direct neighbors. Via the connection of this Markov network, the sampled shadow and non shadow PVs are formed to build a shadow libraryL_S and a non shadow libraryL_N, respectively, as shown in the training stage in Fig. 1.

IV EXPERIMENTS AND RESULTS

In our experiments, we evaluate both shadow detection and shadow removal results. For shadow recognition, we

evaluate how explicitly modelling the pair-wise region association affects detection results and the performance of our detector can oversimplify cross datasets. For shadow removal, we evaluate the results quantitatively on our dataset by comparing the recovered image with the shadow-free ground truth and

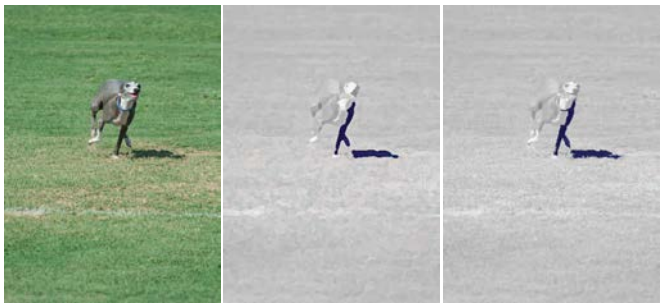

Fig. 5Illustration of WV-2 image. (a) Original image with shadows. (b) Shadow detected image of paired region based method (c) Shadow detected image of morphological filtering and edge compensation. filtering and edge compensation are shown in Figs. 6(c), 7(c), and 8(c), respectively, from which we can observe that the main and correct shadow regions are preserved and that the penumbra effects caused by high-brightness surroundings along the shadow direction are compensated, such as the gray areas in red polygons of Fig. 8 (c).

V CONCLUSION

This paper compares the shadow detection algorithm based on morphological operation and paired region on the basis of shadow detection methods. For shadow detection, from side to side paired region based algorithm that pair-wise relationships among regions offer valuable additional information about the illumination situation of regions that applies the soft matting to the detection results, the lighting conditions for each pixel in the image are improved reflected, especially for pixels which are on the boundary of shadow areas. While MF based technique combines the shadow properties and spectral characteristics of objects, to utilize thresholding method and morphological filtering to detect shadows. The results derived shadow region is unbroken and transitions between shadow and nonshadow regions are cautiously considered, the superiorities of the proposed one are there is no need a classification step, it allows within class variations for one land-cover type by only selecting those candidates that are mainly analogous to the study pixel, and it keeps good compatibility between the reconstructed shadow regions and their surrounding nonshadow regions.

REFERENCES

[1] J. Zhu, K.G.G. Samuel, S. Masood, and M.F. Tappen, "Learning to Recognize Shadows in Monochromatic Natural Images," Proc. IEEE Conf. Computer Vision and Pattern Recognition, 2010.

[2] J.-F. Lalonde, A.A. Efros, and S.G. Narasimhan, "Estimating Natural Illumination from a Single Outdoor Image," Proc. 12th IEEE Int'l Conf. Computer Vision, 2009.

[3] K. Karsch, V. Hedau, D. Forsyth, and D. Hoiem, "Rendering Synthetic Objects Into Legacy Photographs," Proc. ACM Siggraph, 2011.

[4] D.L. Waltz, "Generating Semantic Descriptions from Drawings of Scenes with Shadows," technical report, 1972.

[5] H. Barrow and J. Tenenbaum, "Recovering Intrinsic Scene Characteristics from Images," Computer Vision Systems, pp. 3-26, 1978.

[6] J.-F. Lalonde, A.A. Efros, and S.G. Narasimhan, "Detecting Ground Shadows in Outdoor Consumer Photographs," Proc. 11th European Conf. Computer Vision, 2010.

[7] M. Mokhtarzade and M. J. V. Zoej, "Road detection from high-resolution satellite images using artificial neural networks," Int. J. Appl. Earth Observ. Geoinf., vol. 9, no. 1, pp. 32–40, Feb. 2007.

[8] K. Johansen, N. C. Coops, S. E. Gergel, and Y. Stange, "Application of high spatial resolution satellite imagery for riparian and forest ecosystem classification," Remote Sens. Environ., vol. 110, no. 1, pp. 29–44, Sep. 2007.

[9] R. Mathieu, C. Freeman, and J. Aryal, "Mapping private gardens in urban areas using object-oriented techniques and very high-resolution satellite imagery," Landscape Urban Plann., vol. 81, no. 3, pp. 179–192, Jun. 2007.

[10] T. Kim, T. Javzandulam, and T.-Y. Lee, "Semiautomatic reconstruction of building height and footprints from single satellite images," in Proc. IEEE IGARSS, Jul. 2007, vol. 2, pp. 4737–4741.

[11] P.M. Dare, "Shadow analysis in high-resolution satellite imagery of urban areas," Photogramm. Eng. Remote Sens., vol. 71, no. 2, pp. 169–177, Feb. 2005.

[12] S. Hinz and A. Baumgartner, "Vehicle detection in aerial images using generic features, grouping, and context," in Proc. Pattern Recognit., Lect. Notes Comput. Sci., 2001, vol. 2191, pp. 45–52.

[13] A. K. Shackelford, C. H. Davis, and X. Wang, "Automated 2-D building footprint extraction from high-resolution satellite multispectral imagery," in Proc. IEEE IGARSS, Sep. 2004, vol. 3, pp. 1996–1999.

[14] J. Liu, J. Yang, and T. Fang, "Color property analysis of remote sensing imagery," Acta Photon. Sinica, vol. 38, no. 2, pp. 441–447, Feb. 2009.

[15] H. Ma, Q. Qin, and X. Shen, "Shadow segmentation and compensation in high resolution satellite images," in Proc. IEEE IGARSS, Jul. 2008, vol. 2, pp. 1036–1039.

[16] V. Tsai, "A comparative study on shadow compensation of color aerial images in invariant color models," IEEE Trans.

Geosci. Remote Sens., vol. 44, no. 6, pp. 1661–1671, Jun. 2006.

[17] L. Lorenzi, F. Melgani, and G. Mercier, "A complete processing chain for shadow detection and reconstruction in VHR images," IEEE Trans. Geosci. Remote Sens., vol. 50, no. 9, pp. 3440–3452, Sep. 2012.

[18] F. Yamazaki, W. Liu, and M. Takasaki, "Characteristics of shadow and removal of its effects for remote sensing imagery," in Proc. IEEE IGARSS, Jul. 2009, vol. 4, pp. 426–429.

[19] A. Levin, D. Lischinski, and Y. Weiss, "A Closed-Form Solution to Natural Image Matting," IEEE Trans. Pattern Analysis and Machine Intelligence, vol. 30, no. 2, pp. 228-242, Feb. 2008.

[20] D.R. Martin, C. Fowlkes, and J. Malik, "Learning to Detect Natural Image Boundaries Using Local Brightness, Color, and Texture Cues," IEEE Trans. Pattern Analysis and Machine Intelligence, vol. 26, no. 5, pp. 530-549, May 2004.

[21] C.-C. Chang and C.-J. Lin, "LIBSVM: A Library for Support Vector Machines," ACM Trans. Intelligent Systems and Technology, vol. 2, pp. 27:1-27:27, 2011.

[22] M. Baba and N. Asada, "Shadow Removal from a Real Picture," Proc. ACM Siggraph, 2003.

[23] V. Kolmogorov and R. Zabih, "What Energy Functions Can Be Minimized via Graph Cuts," IEEE Trans. Pattern Analysis and Machine Intelligence, vol. 26, no. 2, pp. 65-81, Feb. 2004.

[24] M. Nagao, T. Matsutyama, and Y. Ikeda, "Region extraction and shape analysis in aerial photos," Comput. Graph. Image Process., vol. 10, no. 3, pp. 195–223, Jul. 1979.

[25] P. Maragos, The Image and Video Processing Handbook, 2nd ed. New York, NY, USA: Elsevier, 2005, pp. 135–156.

[26] R. Trias-Sanz and N. Loménìe, "Automatic bridge detection in highresolution satellite images," in Proc. Comput. Vis. Syst. Lect. Notes Comput. Sci., 2003, vol. 2626, pp. 172–181.

[27] A. Katartzis and H. Sahli, "A stochastic framework for the identification of building rooftops using a single remote sensing image," IEEE Trans. Geosci. Remote Sens., vol. 46, no. 1, pp. 259–271, Jan. 2008.

[28] Y. Yang, C. Han, and D. Han, "AMarkov random field model-based fusion approach to segmentation of SAR and optical images," in Proc. IEEE IGARSS, Jul. 2008, vol. 4, pp. 802–805.

[29] Ruiqi Guo, Qieyun Dai and Derek Hoiem Paired Regions for Shadow Detection and Removal IEEE TRANSACTIONS ON PATTERN ANALYSIS AND MACHINE INTELLIGENCE, VOL. 35, NO. 12, DECEMBER 2013.

[30] Huihui Song, Bo Huang and Kaihua Zhang "Shadow Detection and Reconstruction in High-Resolution Satellite Images via Morphological Filtering and Example-Based Learning" IEEE TRANSACTIONS ON GEOSCIENCE AND REMOTE SENSING, VOL. 52, NO. 5, MAY 2014.